JOC Article

Model Studies of 6,7-Indolequinone Cofactors of Quinoprotein Amine Dehydrogenases

Yoko Murakami,[†] Noriyuki Yoshimoto,[†] Nobutaka Fujieda,[‡] Kei Ohkubo,[§] Tatsuhiko Hasegawa,[†] Kenji Kano,*[,‡] Shunichi Fukuzumi,*[,§] and Shinobu Itoh*[,†]

Department of Chemistry, Graduate School of Science, Osaka City University, 3-3-138 Sugimoto, Sumiyoshi-ku, Osaka 558-8585, Japan, Department of Material and Life Science, Graduate School of Engineering, Osaka University, 2-1 Yamada-oka, Suita, 565-0871 Osaka, Japan, and Division of Applied life Science, Graduate School of Agriculture, Kyoto University, Sakyo-ku, Kyoto 606-8502, Japan

shinobu@sci.osaka-cu.ac.jp; fukuzumi@chem.eng.osaka-u.ac.jp; kkano@kais.kyoto-u.ac.jp

Received January 6, 2007

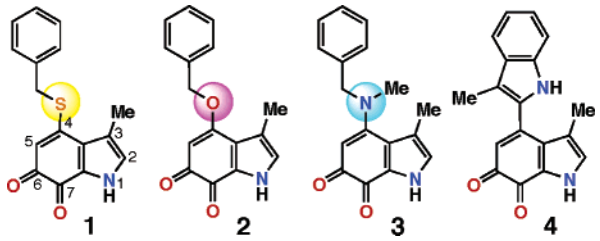

The electronic effects of the C-4 substituent on the physicochemical properties and reactivity of the 6,7-inodolequinone cofactors (CTQ and TTQ) have extensively been investigated with use of a series of C-4 substituted 6,7-inodolequinone derivatives (**1**−**4**). The one-electron reduction potentials of the 6,7-inodolequinone derivatives decrease with increasing the electron donating ability of the C-4 substituent (with the following order of $E^{\circ\prime}$: **4** > **1** > **2** > **3**). The reaction of indolequinones **1**−**3** with benzylamine proceeds *stepwise* through the iminoquinone and the product-imine intermediates to give aminophenol as the final product as the case of TTQ model compound **4**. The rate constants of each step have been determined by the detailed kinetic analysis, and the kinetic deuterium isotope effects have also been examined to confirm the rate-determining step. The reactivity of CTQ model compound **1** toward the amines is by one order of magnitude lower than that of TTQ model compound **4**. The reactivity of indolequinones **2** and **3** is further decreased due to their stronger electron-donating substituents at C-4. A more important difference between CTQ model compound **1** and TTQ model compound **4** is the reactivity of the iminoquinone intermediate: the reaction of the CTQ model compound with amines stops at the iminoquinone formation stage *at room temperature*, whereas the reaction of the TTQ model compound with amines proceeds up to the aminophenol formation. Thus, the energy barrier for the rearrangement of the iminoquinone to the product-imine is higher in the CTQ model system than in the TTQ model system.

Introduction

The redox enzymes containing an organic quinone cofactor are called *quinoprotein*. The first example of such an enzyme is methanol dehydrogenase of methylotrophic bacteria, which involves pyrroloquinolinequinone (PQQ, Figure 1) as the coenzyme.[1,2] Since then, PQQ has been identified as the redox coenzyme of several bacterial dehydrogenases such as glucose dehydrogenases and alcohol dehydrogenases.[3−5] PQQ has also received recent attention as a novel vitamin B in mammals.[6] PQQ is derived from a peptide precursor containing conserved

* Address correspondence to these authors.
[†] Osaka City University.
[§] Osaka University.
[‡] Kyoto University.

(1) Salisbury, S. A.; Forrest, H. S.; Cruse, W. B.; Kennard, O. *Nature* **1979**, *280*, 843−844.
(2) Duine, J. A.; Frank, J., Jr.; Van Zeeland, J. K. *FEBS Lett.* **1979**, *108*, 443−446.
(3) Anthony, C. *Antioxid. Redox Signaling* **2001**, *3*, 757−774.
(4) Anthony, C. *Arch. Biochem. Biophys.* **2004**, *428*, 2−9.
(5) Toyama, H.; Mathews, F. S.; Adachi, O.; Matsushita, K. *Arch. Biochem. Biophys*. **2004**, *428*, 10−21.
(6) Kasahara, T.; Kato, T. *Nature* **2003**, *422*, 832.

10.1021/jo0700272 CCC: $37.00
Published on Web 03/28/2007

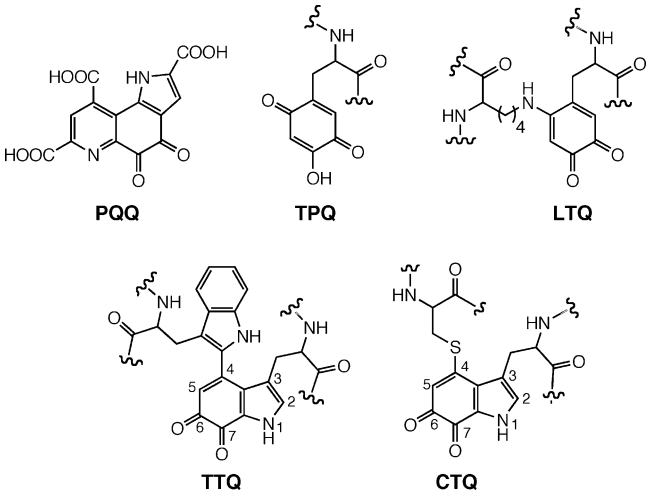

FIGURE 1. Quinone cofactors.

glutamate and tyrosine residues,[7−10] being weakly bound to the active site of the enzymes via ionic interactions through its three carboxylate groups. Thus, PQQ is dissociable into solution.

The second class of quinoprotein consists of copper-containing amine oxidases and lysyl oxidase, which involve tyrosine-derived cofactors, 2,4,5-trihydroxyphenylalanine quinone (TPQ)[11] and lysine tyrosylquinone (LTQ),[12] respectively (Figure 1).[13,14] Formation of these quinone cofactors from the tyrosine precursor requires only a cupric ion and O_2, indicating that the post-translational modification of tyrosine is a self-processing reaction (self-catalysis requiring no external enzyme).[15−19] In contrast to PQQ, TPQ and LTQ cofactors are tightly bound to the peptide backbones of the enzymes. Thus, these cofactors are difficult to isolate intact from the enzyme matrix.

TTQ (tryptophan tryptophylquinone) and CTQ (cysteine tryptophylquinone) constitute the third class of quinone cofactors, which were discovered from methylamine and aromatic amine dehydrogenases and quinohemoprotein amine dehydrogenases, respectively.[20−22] As can be easily recognized from their common indolequinone structure, TTQ and CTQ are derived post-translationally from an active site tryptophan. Thus, they are also bound to the enzyme matrix through the peptide bonds. In contrast to TPQ and LTQ, however, biogenesis of TTQ is more complicated and requires external enzymes such as *c*-type heme proteins.[23,24]

TTQ has a 2-indolyl group originating from another tryptophan residue in the enzyme active site, whereas CTQ forms a thioether linkage with the nearby cysteine in the enzyme active site (Figure 1). In spite of having different C-4 substituents, both TTQ and CTQ catalyze oxidative deamination of primary amines to the corresponding aldehydes (eq 1). Davidson and

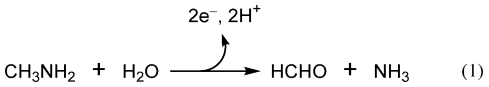

(1)

co-workers demonstrated that the mutation of Trp108 of the β-subunit of methylamine dehydrogenase to cysteine and histidine resulted in formation of CTQ and histidine tryptophylquinone cofactors, respectively.[25] Then, important questions arise: why do these enzymes employ the redox cofactors with different C-4 substituents and how do the C-4 substituents affect the intrinsic reactivity of the 6,7-inolequinones? To answer such questions, it is necessary to study the redox reactivity of a series of TTQ and CTQ model compounds.

We report herein the first systematic study on the amine-oxidation with a series of 6,7-indolequinones (**1**−**3**) to examine the effects of C-4 substituents on the structure and the redox reactivity of the 6,7-indolequinone cofactors. Since we have previously examined the amine-oxidation with the TTQ model compounds (**4**−**6** in Chart 1),[26−28] the present study provides an excellent opportunity to clarify the difference in the redox reactivity between CTQ and TTQ cofactors with different C-4 substituents and gives valuable insight into the enzymatic functions and mechanisms of the 6,7-indolequinone cofactors.

Results and Discussion

Synthesis. CTQ model compound **1** was prepared by the Michael addition of benzyl mercaptan to 3-methyl-1-*p*-tosylindole-6,7-dione **7** as a key step.[29] This strategy was adopted to the synthesis of **2** and **3** as shown in Scheme 1. Thus, the reaction of **7** and benzyl alcohol in the presence of potassium *tert*-butoxide and the following workup treatment under aerobic conditions (in the presence of O_2) gave the expected quinone

(7) Goosen, N.; Huinen, G. R. M.; van de Putte, P. *J. Bacteriol.* **1992**, *174*, 1426−1427.
(8) Houck, D. R.; Hanners, J. L.; Unkefer, C. J. *J. Am. Chem. Soc.* **1988**, *110*, 6920−6921.
(9) Houck, D. R.; Hanners, J. L.; Unkefer, C. J. *J. Am. Chem. Soc.* **1991**, *113*, 3162−3166.
(10) Magnusson, O. T.; Toyama, H.; Saeki, M.; Schwarzenbacher, R.; Klinman, J. P. *J. Am. Chem. Soc.* **2004**, *126*, 5342−5343.
(11) Janes, S. M.; Mu, D.; Wemmer, D.; Smith, A. J.; Kaur, S.; Maltby, D.; Burlingame, A. L.; Klinman, J. P. *Science* **1990**, *248*, 981−987.
(12) Wang, S. X.; Mure, M.; Medzihradszky, K. F.; Burlingame, A. L.; Brown, D. E.; Dooley, D. M.; Smith, A. J.; Kagan, H. M.; Klinman, J. P. *Science* **1996**, *273*, 1078−1084.
(13) Dove, J. E.; Klinman, J. P. *Adv. Protein Chem.* **2001**, *58*, 141−174.
(14) Mure, M. *Acc. Chem. Res.* **2004**, *37*, 131−139.
(15) Nakamura, N.; Matsuzaki, R.; Choi, Y.-H.; Tanizawa, K.; Sanders-Loehr, J. *J. Biol. Chem.* **1996**, *271*, 4718−4724.
(16) Ruggiero, C. E.; Smith, J. A.; Tanizawa, K.; Dooley, D. M. *Biochemistry* **1997**, *36*, 1953−1959.
(17) Bollinger, J. A.; Brown, D. E.; Dooley. D. M. *Biochemistry* **2005**, *44*, 11708−11714.
(18) Okeley, N. M.; van der Donk, W. A. *Chem. Biol.* **2000**, *7*, R159−R171.
(19) DuBois, J. L.; Klinman, J. P. *Arch. Biochem. Biophys.* **2005**, *433*, 255−265.
(20) Mclntire, W. S.; Wemmer, D. E.; Chistoserdov, A.; Lidstrom, M. E. *Science* **1991**, *252*, 817−824.
(21) Datta, S.; Mori, Y.; Takagi, K.; Kawaguchi, K.; Chen, Z. W.; Okajima, T.; Kuroda, S.; Ikeda, T.; Kano, K.; Tanizawa, K.; Mathews, F. S. *Proc. Natl. Acad. Sci. U.S.A.* **2001**, *98*, 14268−14273.
(22) Satoh, A.; Kim, J. K.; Miyahara, I.; Devreese, B.; Vandenberghe, I.; Hacisalihoglu, A.; Okajima, T.; Kuroda, S.; Adachi, O.; Duine, J. A.; Van Beeumen, J.; Tanizawa, K.; Hirotsu, K. *J. Biol. Chem.* **2002**, *277*, 2830−2834.
(23) Wang, Y. T.; Graichen, M. E.; Liu, A. M.; Pearson, A. R.; Wilmot, C. M.; Davidson, V. L. *Biochemistry* **2003**, *42*, 7318−7325.
(24) Wang, Y.; Li, X.; Jones, L. H.; Pearson, A. R.; Wilmot, C. M.; Davidson, V. L. *J. Am. Chem. Soc.* **2005**, *127*, 8258−8259.
(25) Pearson, A. R.; Jones, L. H.; Higgins, L.; Ashcroft, A. E.; Wilmot, C. M.; Davidson, V. L. *Biochemistry* **2003**, *42*, 3224−3230.
(26) Itoh, S.; Ogino, M.; Haranou, S.; Terasaka, T.; Ando, T.; Komatsu, M.; Ohshiro, Y.; Fukuzumi, S.; Kano, K.; Takagi, K.; Ikeda, T. *J. Am. Chem. Soc.* **1995**, *117*, 1485−1493.
(27) Itoh, S.; Takada, N.; Haranou, S.; Ando, T.; Komatsu, M.; Ohshiro, Y.; Fukuzumi, S. *J. Org. Chem.* **1996**, *61*, 8967−8974.
(28) Itoh, S.; Takada, N.; Ando, T.; Haranou, S.; Huang, X.; Uenoyama, Y.; Ohshiro, Y.; Komatsu, M.; Fukuzumi, S. *J. Org. Chem.* **1997**, *62*, 5898−5907.
(29) Murakami, Y.; Tachi, Y.; Itoh, S. *Eur. J. Org. Chem.* **2004**, 3074−3079.

CHART 1

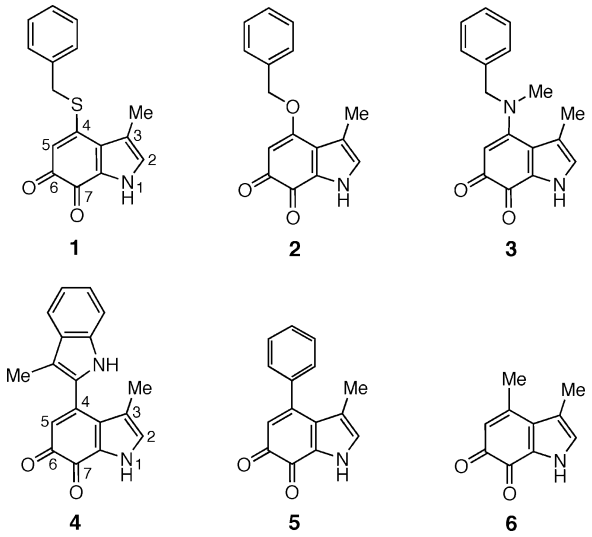

SCHEME 1

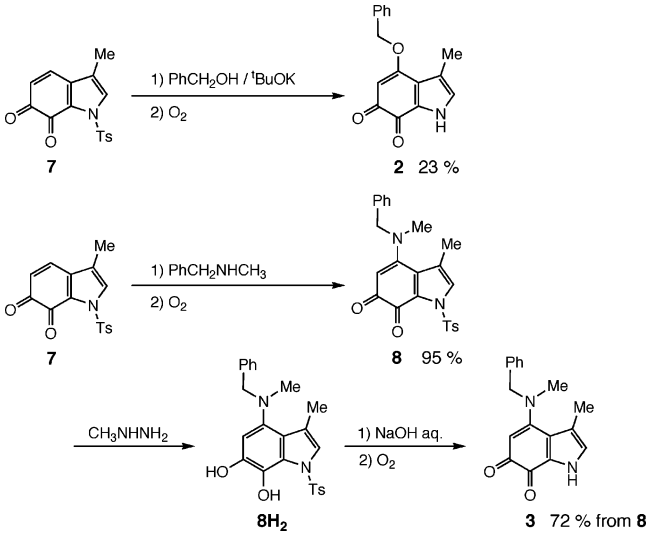

product **2** in a 23% isolated yield. In this reaction, *tert*-butoxide led to simultaneous deprotection of the tosyl group to give the final product **2** directly from **7**.

In the case of *N*-methylbenzylamine, the Michael addition reaction proceeded smoothly even in the absence of the strong base to give quinone **8**, where the *N*-tosyl group remained. Thus, deprotection of the tosyl group from **8** was performed on the hydroquinone derivative $\mathbf{8H_2}$ (prepared by the reduction of **8** with CH_3NHNH_2) by an alkaline treatment with 3 N NaOH in $H_2O-EtOH$ (9:5, v/v). An ordinary workup treatment followed by SiO_2 column chromatography under aerobic conditions gave the expected quinone product **3** in a fairly good yield.

Structural Characterization. In the previous study, the crystal structures of synthetic intermediates **7** and **9** (see Chart 2) were determined to obtain an important insight into the electronic effect of the thioether substituent at C-4.[29] In this study, the crystal structures of **3** and **8** have also been determined, and were also compared to those of **7** and **9** as shown in Figure 2. The crystallographic data and the selected bond lengths and angles are presented in Tables S1 and S2 (see the Supporting Information).

It was previously pointed out that the bond length of C(5)−C(6) (1.437 Å) in **9** is shorter than that in **7** (1.468 Å), while

CHART 2

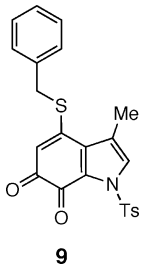

SCHEME 2

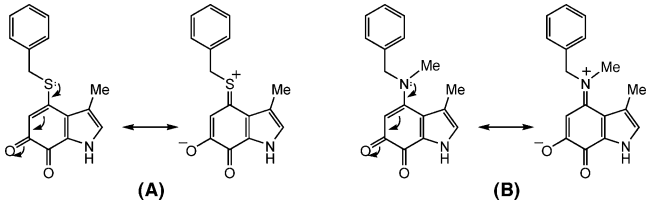

the bond lengths of C(4)−C(5) and C(6)−O(1) in **9** (1.357 and 1.221 Å, respectively) are longer than those in **7** (1.337 and 1.215 Å, respectively).[29] Moreover, the bond length of S(1)−C(4) (1.720 Å) in **9** is slightly shorter than the typical S−C bond length in simple thioanisole derivatives (1.77 Å).[30,31] These structural features clearly indicate that there exists a conjugative interaction between S(1) and the α,β-unsaturated carbonyl moiety [C(4)═C(5)−C(6)═O(1)] of compound **9** as illustrated in Scheme 2A.

The bond length of C(5)−C(6) (1.427 Å) in **8** is further shortened as compared to that in **9** (1.437 Å), whereas the bond lengths of C(4)−C(5) and C(6)−O(1) in **8** (1.380 and 1.243 Å, respectively) are elongated as compared to those in **9** (1.357 and 1.221 Å, respectively) because of the stronger conjugative interaction between the C-6 quinone carbonyl group and the C-4 substituent (Scheme 2B). On the other hand, it is apparent that the electronic effect of the *p*-tosyl group on N-1 is not so significant judging from the similar bond lengths of the *o*-quinone ring between **3** and **8**. In spite of our great efforts, single crystals of **1**, **2**, and **4** suitable for X-ray crystallographic analysis have yet to be obtained.

IR and UV−Vis Spectra. The C═O stretching vibration of the 6,7-indolequinone derivatives is summarized in Table 1 (the whole spectra of **1**−**4** are presented in the Supporting Information, Figures S1−S4).

The C-4 heteroatom-substituted derivatives **1**−**3** exhibit two distinct peaks at around 1660 and 1600 cm^{-1}, which can be assigned to the C═O stretching vibration of the quinone carbonyl groups at C-7 and C-6, respectively. On the other hand, only a strong peak is observed at 1629 cm^{-1} in the case of **4**. With respect to the IR data of **1**−**3**, the C═O stretching vibration energy of the C-7 quinone carbonyl group is relatively constant (1661−1663 cm^{-1}), whereas that of the C-6 quinone carbonyl group of **3** (1595 cm^{-1}) is significantly lower that those of **1** and **2** (1630 and 1631 cm^{-1}, respectively). This result may be attributed to the stronger conjugative interaction between the C-6 carbonyl group and the amino group in **3** (Scheme 2B) as compared to the conjugation between the C-6 carbonyl group and the thioether group in **1** (Scheme 2A). The larger contribu-

(30) Abramovitch, R. A.; Ye, X. C.; Pennington, W. T.; Schimek, G.; Bogdal, D. *J. Org. Chem.* **2000**, *65*, 343−351.
(31) Brunner, H.; Mijolovic, D.; Zabel, M. *Synthesis* **2001**, 1671−1680.

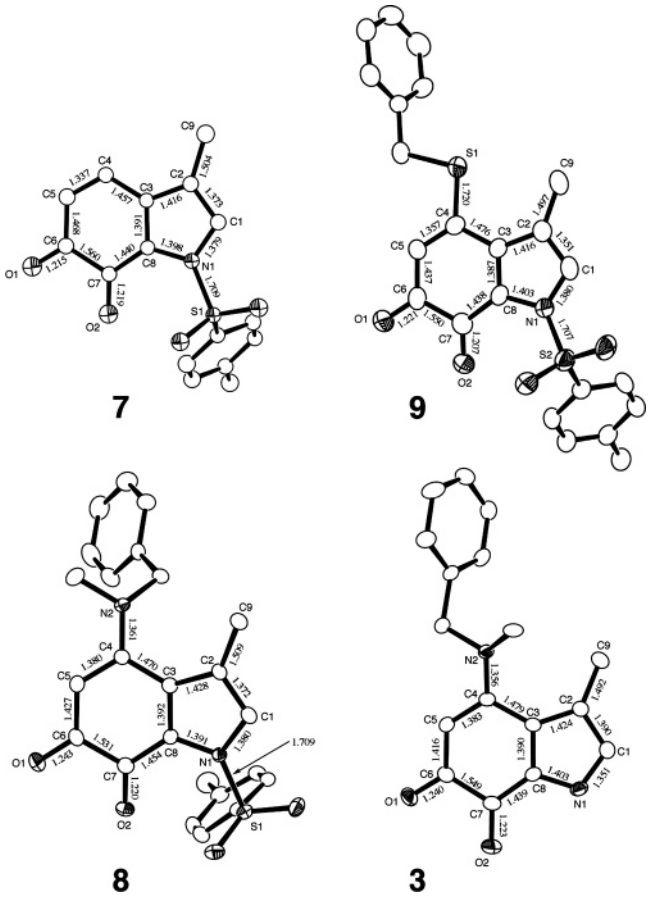

FIGURE 2. ORTEP drawings of compounds **3**, **7**, **8**, and **9** showing 50% probability thermal ellipsoids. The hydrogen atoms are omitted for simplicity. The ORTEP drawings of **7** and **9** are generated with the data reported in ref 29. The selected bond lengths (Å) are also indicated.

tion of the *p*-quinonoid resonance form (the twitter anionic form) would decrease the bond order of the carbonyl group at C-6 as depicted in Scheme 2, thus lowering the C═O stretching vibration energy at C-6. Judging from the similarity in the IR data between **1** and **2**, the degree of conjugation between the C-6 carbonyl group and the ether group in **2** may be similar to that between the C-6 carbonyl group and the thioether group in **1**. In the case of **4**, the conjugation between the C-6 quinone carbonyl group and the C-4 aromatic substituent may be smaller than that in **1**−**3**. Thus, the conjugation between the C-6 and C-7 quinone carbonyl groups becomes stronger, giving rise to only one intense C═O bond vibration peak at 1629 cm^{-1}.

The UV−vis spectra of the 6,7-indolequinone derivatives are presented in Figure 3. The λ_{max} values and the molar absorption coefficient ϵ (M^{-1} cm^{-1}) of the quinones are also listed in Table 1. The CTQ model compound **1** exhibits an intense absorption band at 343 nm together with a shoulder around 380 nm, which can be attributed to the $\pi-\pi^*$ transition of the *o*-quinone ring. In addition, there is a weak and broad band at 450−600 nm (ϵ = 920 M^{-1} cm^{-1}), which may be assigned to the $n-\pi^*$ transition of the *o*-quinone moiety. These absorption bands are very similar to those of native CTQ, 350−380 nm ($\pi-\pi^*$) and 450−600 nm ($n-\pi^*$), although the absorption band around 350 nm of native CTQ is not well separated from the band at 380 nm.[29,32]

Compounds **2** and **3** also exhibit the $\pi-\pi^*$ transition band at 375 and 372 nm, respectively, together with the $n-\pi^*$ transition band in a similar region (450−600 nm). These absorption bands in the visible region of **1**−**3** are blue-shifted as compared to those of TTQ model compound **4** ($\pi-\pi^*$: 407 nm, ϵ = 8500 M^{-1} cm^{-1}; $n-\pi^*$: 500−650 nm).[26]

Reduction of the quinones to the corresponding quinol derivatives by $MeNHNH_2$ resulted in the disappearance of the visible absorption bands, and instead a new intense absorption band appeared blow 350 nm as shown in Figure 4. Thus, the color of the solution of the reduced compound becomes pale yellow. These spectral changes observed upon reduction are also similar to those of native cofactors TTQ and CTQ in the enzymatic systems.[32−34]

Electrochemistry. Figure 5 shows a cyclic voltammogram of **1** (pH 6.8) at a scan rate (υ) of 10 mV s^{-1} as a typical example. Compound **1** gave a pair of cathodic and anodic waves and the peak currents increase proportional to υ. This indicates that the quasireversible characteristic is ascribed to the adsorbed species of compound **1**. The pH dependence of the midpoint potential (formal potential, $E^{\circ\prime}$) is depicted in Figure 6 (closed circles). The $E^{\circ\prime}$ vs pH profile is composed of three straight lines with slopes of −60 mV/pH (pH < 8), −30 mV/pH (8.5 < pH < 10.5), and −60 mV/pH (pH > 11). It is well-known that the slope is given by $-2.303mRT/nF$ for a ne^--mH^+ process (F is the Faraday constant and $-2.303RT/F$ is −60 mV at 25 °C). Since the number of electrons (n) involved in the electrode reactions is 2 in the present case, the slope indicates that the electrode reaction is a $2e^-$-$2H^+$ process below pH 8, a $2e^-$-$1H^+$ process in the range from pH 8.5 to 10.5, and a $2e^-$-$2H^+$ process above pH 11. This pH profile is very similar to that of **4** in the previous study,[26] and the inflection point appearing at pH 10.4 corresponds to the pK_a of the oxidized form of compound **1** due to the dissociation of 1-NH as in the case with compound **4** (Table 1). The pK_a value of **1** thus determined electrochemically agrees well with that obtained independently from the spectral titration (10.9) in Figure S5. The other inflection point at pH 8.3 corresponds to the pK_a of the reduced form of compound **1** due to the dissociation of the phenolic OH group (Table 1). The pK_a value is much smaller than that of compound **4** (pK_a = 10.1), but the value agrees well with that of CTQ bound to the γ subunit polypeptides, which is isolated from the native QH-AmDHs.[32]

Although the $E^{\circ\prime}$ value of **2** is more negative than that of **1** (∼80 mV), the $E^{\circ\prime}$ vs pH profile is very similar to that of **1** with two inflection points at pH 8.4 and 10.4 (Figure 6, triangles, and Table 1). The same pK_a values (10.4) of the pyrrolic protons (1-NH) in **1** and **2** suggest that the conjugative interaction between the C-4 substituents and the five-membered (pyrrole) ring is negligible. On the other hand, the similar pK_a values of the phenolic protons in the quinol derivatives $\mathbf{1H_2}$ and $\mathbf{2H_2}$ suggest that the electronic effect of the C-4 substituents in the reduced form is very small, because they are separated by four atoms ($X-C_4-C_5-C_6-O_6$).

The $E^{\circ\prime}$ value of **3** is slightly negative as compared with that of **2**. However, the $E^{\circ\prime}$ vs pH profile of **3** is composed of four straight lines with three inflection points at 5.6, 8.4, and 10.6 (Figure 6, open circles). The slope of the additional line was −90 mV/pH below pH 6, where a $2e^-$-$3H^+$ electrode reaction occurred. The inflection point at pH 5.6 corresponds to pK_a of

(32) Fujieda, N.; Mori, M.; Kano, K.; Ikeda, T. *Biochemistry* **2002**, *41*, 13736−13743.
(33) Kenney, W. C.; McIntire, W. *Biochemistry* **1983**, *22*, 3858−3868.
(34) Husain, M.; Davidson, V. L. *Biochemistry* **1987**, *26*, 4139−4143.

TABLE 1. Physicochemical Properties of 6,7-Indolequinone Derivatives

	1[a]	**2**	**3**	**4**[a]
FT-IR, $\nu_{(C=O)}$/cm^{-1}	1663 (C-7) 1630 (C-6)	1662 (C-7) 1631 (C-6)	1661 (C-7) 1595 (C-6)	1629
λ_{max} (ϵ/M^{-1} cm^{-1})	343 (14800) 380 (12000)	375 (12500)	372 (9900) 514 (770)	407 (8500) 550 (1600)
pK_a, 1-NH	10.4	10.4	10.6	10.9[b]
OH in reduced form	8.3	8.4	8.4	10.1[b]
$E^{\circ\prime}$ vs Ag|AgCl (mV)[c]	−190	−273	−307	−90

[a] The spectral data of **1** and **4** were retaken in this study under the same conditions. Thus, the data are slightly different from the previous ones.[26,29] [b] Taken in aqueous buffers containing 20% DMSO.[26] [c] Extrapolated value at pH 7.0.

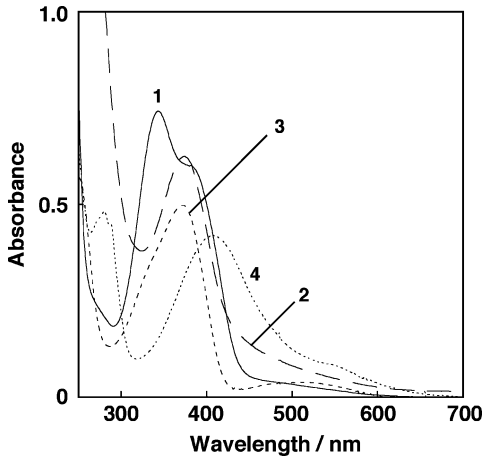

FIGURE 3. UV−vis spectra of **1**, **2**, **3**, and **4** (5.0×10^{-5} M) in CH_3CN at 30 °C.

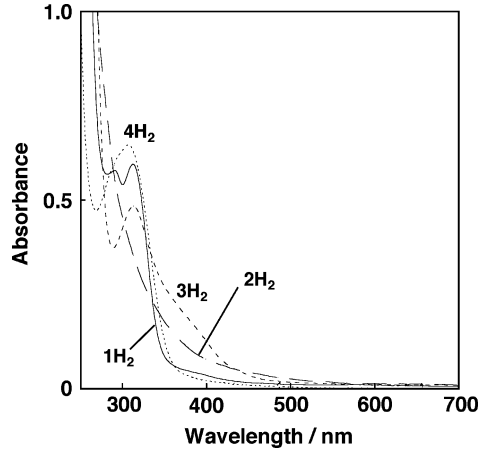

FIGURE 4. UV−vis spectra of **1H$_2$**, **2H$_2$**, **3H$_2$**, and **4H$_2$** (5.0×10^{-5} M) generated by the reduction of the quinones with $MeNHNH_2$ (10−100 equiv) in MeCN at 30 °C.

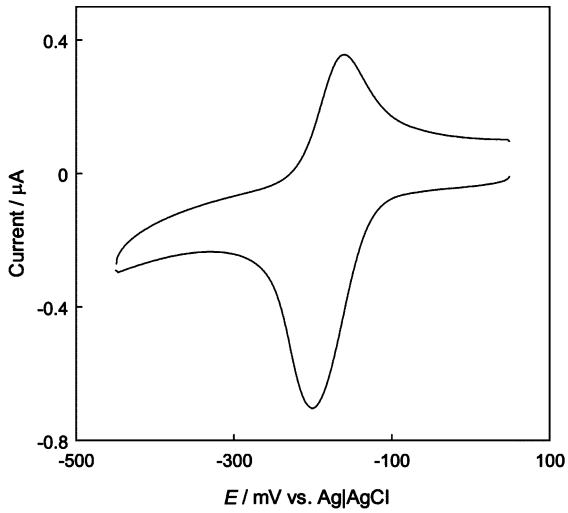

FIGURE 5. Cyclic voltammogram of compound **1** at $\upsilon = 10$ mV s^{-1} in 0.5 M phosphate containing 20% (v/v) isopropyl alcohol and 0.5% DMSO (pH 6.8).

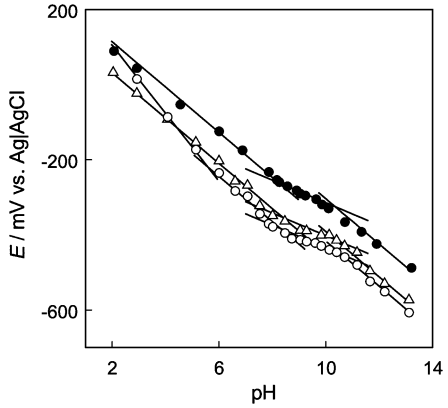

FIGURE 6. $E^{\circ\prime}$ vs pH profiles of compounds **1** (●), **2** (△), and **3** (○).

the reduced and protonated form of **3** due to the dissociation of the protonated tertiary amine moiety. Overall, the replacement of the S atom by O and N causes small effects on the acid−base property of the model compounds.

Reaction of Amines and CTQ Model Compound 1. To obtain detailed insights into the catalytic mechanism of quinohemoprotein amine dehydrogenases, the reactions of the CTQ model compound **1** and a series of amines have been investigated as follows.

Formation of Iminoquinone (IQ). The reactions of **1** and several primary amines $R^1R^2CHNH_2$ were examined in methanol at 30 °C. Figure 7A shows the spectral changes in the reaction of **1** (5.0×10^{-5} M) with an excess of benzylamine ($R^1 = -Ph$, $R^2 = -H$; 5.0×10^{-2} M) as a typical example, where spectrum (a) of the starting material **1** at 352 nm quickly changed to spectrum (b) (within a second) that was then gradually converted to spectrum (c) exhibiting λ_{max} at 337 and 380 nm with a clear isosbestic point at 333 nm. The conversion of spectrum (b) to spectrum (c) obeyed first-order kinetics as shown in the inset of Figure 7A, and the pseudo-first-order rate constant k_{obs} thus obtained was proportional to the amine concentration (Figure 7B). The observed second-order rate constant $k_{obs(2)}$ was determined from the slope of the linear line in Figure 7B.

Similar spectral changes were obtained in the reactions with other amines such as cyclopropylamine ($R^1 = R^2 = -CH_2CH_2-$), *n*-propylamine ($R^1 = -CH_2CH_3$; $R^2 = -H$), cyclo-

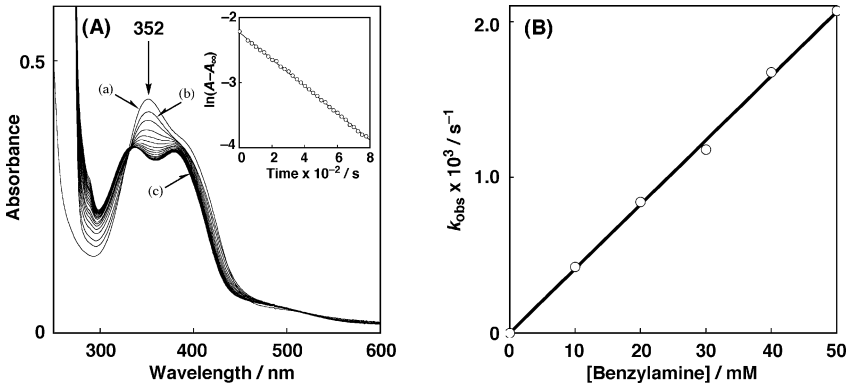

FIGURE 7. (A) Spectral change observed upon addition of benzylamine (5.0×10^{-2} M) to a CH_3OH solution of **1** (5.0×10^{-5} M) at 30 °C. Inset: Pseudo-first-order plot for the iminoquinone formation. (B) Plot of the pseudo-first-order rate constants k_{obs} vs [benzylamine].

TABLE 2. Observed Second-Order Rate Constants ($k_{obs(2)}$) for the Iminoquinone Formation at 30 °C in Methanol and Their UV−Vis Data (λ_{max})[a]

	1		**4**[b]	
amine	λ_{max}/ nm	$k_{obs(2)}$/ M^{-1} s^{-1}	λ_{max}/ nm	$k_{obs(2)}$/ M^{-1} s^{-1}
n-propylamine	334, 378	0.120	402	1.3
benzylamine	337, 380	0.041	400	0.27
cyclopropylamine	385	0.056	392	0.20
cyclohexylamine	334, 376	0.029	391	0.16
isopropylamine	336, 374	0.019	392	0.12
benzhydrylamine		*c*	405	0.0087
tert-butylamine		*c*		*c*

[a] [Quinone] = 5.0×10^{-5} M, in CH_3OH at 30 °C under N_2. [b] Taken from ref 27. [c] Too slow to be determined accurately.

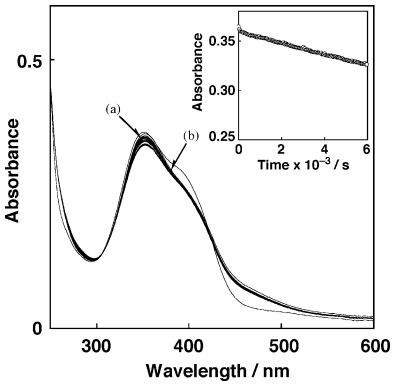

FIGURE 8. Spectral change observed upon addition of *tert*-butylamine (7.5×10^{-2} M) to a CH_3OH solution of **1** (5.0×10^{-5} M) at 30 °C. Inset: Absorbance change at 352 nm.

hexylamine ($R^1 = R^2 = -(CH_2)_5-$), and isopropylamine ($R^1 = -CH_3$; $R^2 = -CH_3$). The $k_{obs(2)}$ values of those amines were determined from the linear plots of the pseudo-first-order rate constants k_{obs} vs the amine concentrations (Figures S6−S9). The spectral data (λ_{max}) of the generated products and the observed second-order rate constants $k_{obs(2)}$ are summarized in Table 2, together with the corresponding data for the reactions of TTQ model compound **4** and the amines.

Figure 8 shows the spectral changes for the reaction of *tert*-butylamine ($^tBuNH_2$) with **1** under the same experimental conditions, where the initial change of spectrum (a) to spectrum (b) was also observed. However, no further reaction is observed at 30 °C.[35] Furthermore, no spectral change was observed in the treatment of **1** with triethylamine (Et_3N) under the same

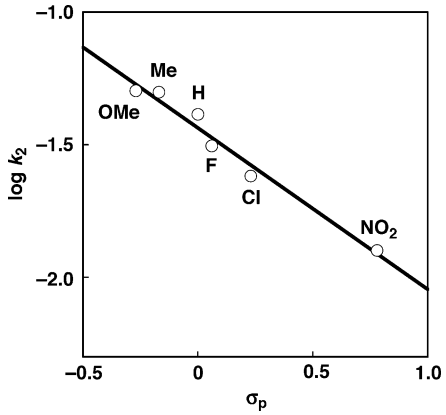

FIGURE 9. Hammett plot for the iminoquinone formation of **1** with *p*-X-$C_6H_4CH_2NH_2$.

conditions, demonstrating that the initial spectral change from (a) to (b) is NOT due to deprotonation of the pyrrole proton (1-NH) of compound **1**. If the spectral change from (a) to (b) were due to the deprotonation of **1**, a similar spectral change should be observed with the stronger base Et_3N. Thus, the first step [spectrum change from (a) to (b)] in Figures 7 and 8 corresponds to an attainment of the equilibrium between quinone **1** and carbinolamine adduct $\mathbf{1_{CA}}^{\mathbf{R1,R2}}$, and the second step [spectrum change from (b) to (c)] in Figure 7 corresponds to the formation of iminoquinone $\mathbf{1_{IQ}}^{\mathbf{R1,R2}}$ from $\mathbf{1_{CA}}^{\mathbf{R1,R2}}$ by dehydration as shown in Scheme 3.

With respect to the addition position of amines to compound **1**, we currently have no direct evidence to support the regiochemistry (C6 vs C7). In the previous model studies of TTQ (**4**), the addition position of C-6 was confirmed by the detailed NMR studies on the isolated iminoquinone derivatives (R^1 = cyclopropyl).[27] In the preparative scale reaction with higher concentration of **1** and cyclopropylamine, however, the amine attached not only to the quinone carbonyl carbons but also to the C-4 carbon, affording a complicated mixture of products. This precluded us to examine the addition position of amines to **1** by the NMR method.[36] Thus, we tentatively assigned C-6 as the addition position of amines based on the DFT study,

(35) The very slow decay of spectrum b in Figure 8 may be due to photoreduction of **1** by the amine in the UV−vis spectrophotometer; cf.: Fukuzumi, S.; Itoh, S.; Komori, T.; Suenobu, T.; Ishida, A.; Fujitsuka, M.; Ito, O. *J. Am. Chem. Soc.* **2000**, *122*, 8435−8443.

(36) Comounds **2** and **3** also provided a complicated mixture of products in the preparative scale reaction with cyclopropylamine.

SCHEME 3

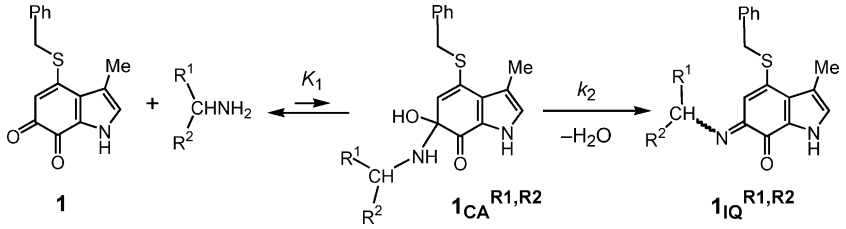

SCHEME 4

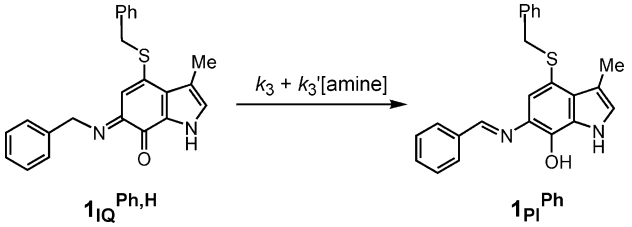

where the calculated atomic charge on the C-6 carbon of **1** (+0.41) was more positive than that on the C-7 carbon (+0.36). A definite conclusion of the regiochemistry needs to wait more detailed theoretical studies.

ESI-MS (positive mode) analysis of the reaction mixture (Figure S10) supports the mechanism in Scheme 3. The starting material **1** gave intense mass peaks at 306 and 589 nm (Figure S10A), and the peak positions and the isotope distribution patterns agree with the chemical formulations of $[\mathbf{1} + Na]^+$ and $[2 \times \mathbf{1} + Na]^+$, respectively. After the reaction with an alkylamine such as cyclopropylamine was completed at room temperature, these peaks disappeared, and new peaks at 323, 345, and 667 nm appeared [Figure S10B]. These peaks can be assigned to $[\mathbf{1_{IQ}}^{Cp} + H^+]^+$, $[\mathbf{1_{IQ}}^{Cp} + Na]^+$, and $[2 \times \mathbf{1_{IQ}}^{Cp} + Na]^+$, respectively (Cp = cyclopropyl).

According to the mechanism in Scheme 3, the kinetic equation is given by eq 2, where K_1 is the equilibrium constant between quinone **1** and carbinolamine adduct $\mathbf{1_{CA}}^{R1,R2}$, and k_2 is the rate constant for the dehydration process from $\mathbf{1_{CA}}^{R1,R2}$ to iminoquinone $\mathbf{1_{IQ}}^{R1,R2}$.

$$v = \frac{k_2 K_1[\text{amine}]}{1 + K_1[\text{amine}]}[\mathbf{1}]_T \qquad (2)$$

Under the present experimental conditions, K_1[amine] must be much smaller than unity (K_1[amine] $\ll$ 1), since the spectral difference between (a) and (b) is significantly small. In such a case, the kinetic equation can be simplified as given by eq 3. Thus, the observed second-rate constant $k_{obs(2)}$ is equal to k_2K_1.

$$v = k_2 K_1[\text{amine}][\mathbf{1}]_T \qquad (3)$$

As clearly seen in Table 2, the reactivity of CTQ model compound **1** is one order of magnitude lower than that of TTQ model compound **4** because of the electron-donating nature of the thioether substituent at C-4 in **1**. The nucleophilic attack by the amine to the quinone carbonyl carbon (K_1) may be disfavored by the increasing electron density at C-6 with the sulfur substituent at C-4. Thus, the different reactivity of the amine substrates may be mainly attributed to the difference in steric bulkiness of the alkyl groups (R^1 and R^2) of amines: the smaller the alkyl substituents, the higher the reactivity (Table 2).

The electronic effects of the para-substituents of benzylamine derivatives on the adduct formation process were also examined as summarized in Table S3 (see the Supporting Information). The Hammett plot shown in Figure 9 affords a good linear correlation between $\log k_{obs(2)}$ and σ_p with $\rho = -0.61$. This clearly demonstrates that the reaction increases with increasing the electron-donating ability of the para-substituent. The electron-donating substituents increase the nucleophilicity of the amine nitrogen, resulting in the larger K_1 value for the adduct formation. On the other hand, the dehydration process (k_2), which includes elimination of H_2O ($OH^- + H^+$), may not be affected so much by the C-4 substituents, since the electron-donating substituents may enhance the elimination of OH^- whereas deprotonation (loss of H^+) would be disfavored by electron donation. Namely, the electronic effects of the C-4 substituents may operate oppositely on the elimination of OH^- and on the deprotonation from the added amine nitrogen. In addition, there was no kinetic deuterium isotope effect (KIE) when the deuterated benzylamine ($PhCD_2NH_2$) was employed. This is reasonable, since the adduct formation process does not involve C−H bond dissociation at the benzylic position of the substrate.

Transformation of Iminoquinone (IQ) to Product Imine (PI). Although the iminoquinone adduct $\mathbf{1_{IQ}}^{Ph,H}$ was stable at 30 °C, it was gradually converted into a product imine $\mathbf{1_{PI}}^{Ph}$ at 60 °C as shown in Scheme 4. Formation of the product imine $\mathbf{1_{PI}}^{Ph}$ was supported by the observed ESI-MS (negative mode) peaks at *m*/*z* 371: the peak position and the isotope distribution pattern agree with the chemical formulation of deprotonated product imine $[\mathbf{1_{PI}}^{Ph} - H]^-$ (Figure S11, Supporting Information).

Figure 10A shows the spectral change for the reaction, where spectrum (c) of the iminoquinone intermediate $\mathbf{1_{IQ}}^{Ph,H}$ at 381 nm gradually decreased with a concomitant increase of a new absorption band at 336 nm [spectrum (d)] with a clear isosbestic point at 364 nm. The reaction obeyed first-order kinetics as shown in the inset of Figure 10A, and a plot of the observed first-order rate constant k_{obs} against the benzylamine concentration gave a linear line with an intercept on the *Y*-axis (Figure 10B). The kinetic results can be expressed by eq 4,

$$k_{obs} = k_3 + k_3'[\text{amine}] \qquad (4)$$

where k_3 is the rate constant for the spontaneous rearrangement from iminoquinone $\mathbf{1_{IQ}}^{Ph,H}$ to product imine $\mathbf{1_{PI}}^{Ph}$ and k_3' is the rate constant for the general base-catalyzed rearrangement from $\mathbf{1_{IQ}}^{Ph,H}$ to $\mathbf{1_{PI}}^{Ph}$. In the latter case, the substrate amine itself also acts as the general base catalyst. From the linear plot in Figure 10B, k_3 and k_3' were determined as 3.2×10^{-4} s^{-1} and 5.9×10^{-4} M^{-1} s^{-1}, respectively.

The kinetic deuterium isotope effect (KIE) has also been examined by using $PhCD_2NH_2$ as the substrate (Figure 10B), where KIE values of 1.1 and 3.2 were obtained for the k_3 and

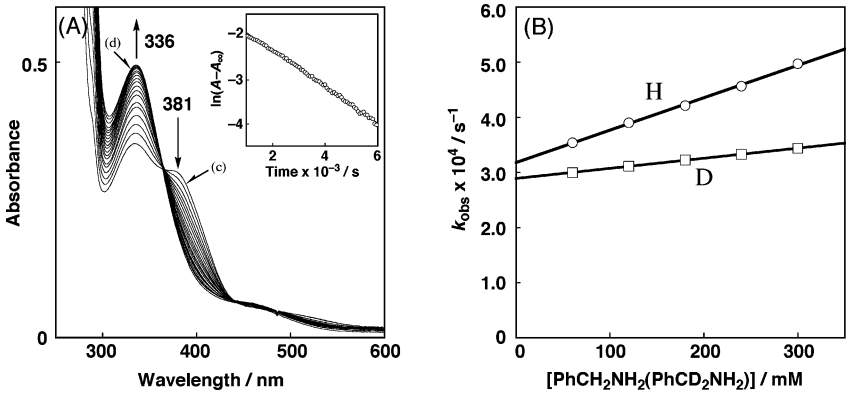

FIGURE 10. (A) Spectral change for the formation of product imine $\mathbf{1_{PI}}^{\mathbf{Ph}}$ from iminoquinone $\mathbf{1_{IQ}}^{\mathbf{Ph,H}}$ generated by the reaction of **1** (5.0×10^{-5} M) and benzylamine (1.8×10^{-1} M) in CH_3OH at 60 °C (isosbestic point: 364 nm.). Inset: Pseudo-first-order plot for the imine intermediate formation. (B) Plots of k_{obs} vs substrate concentration for the formation of product imine $\mathbf{1_{PI}}^{\mathbf{Ph}}$ from iminoquinone $\mathbf{1_{IQ}}^{\mathbf{Ph,H}}$ generated by the reaction of **1** (5.0×10^{-5} M) and benzylamine (1.8×10^{-1} M) in CH_3OH at 60 °C: with $PhCH_2NH_2$ (○) and $PhCD_2NH_2$ (□).

SCHEME 5

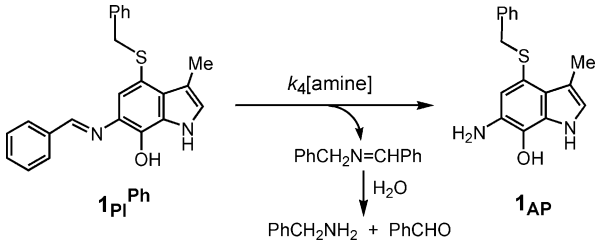

k_3' processes, respectively. Existence of the distinct KIE values is consistent with the mechanism in Scheme 4, which involves rate-limiting benzylic proton migration from the added substrate.

Aminophenol (AP) Formation. Product imine $\mathbf{1_{PI}}^{\mathbf{Ph}}$ was further converted into an aminophenol product $\mathbf{1_{AP}}$ in the prolonged reaction time as shown in Scheme 5. The ESI-MS analysis of the resulting solution after 22 h at 60 °C clearly demonstrated the existence of distinct mass signals around *m*/*z* 283, and the peak position and isotope distribution pattern agree with the formulation of aminophenol $\mathbf{1_{AP}}$ (Figure S12, Supporting Information). In this case, an imine exchange reaction takes place to give $\mathbf{1_{AP}}$ and *N*-benzylidenbenzylamine, the later of which was eventually converted into benzaldehyde and benzylamine by acid-hydrolysis during the workup treatment.

Figure 11A shows the spectral change for the aminophenol formation process, where spectrum (d) due to the product imine intermediate $\mathbf{1_{PI}}^{\mathbf{Ph}}$ is converted into the new spectrum (e) at $\lambda_{max} = 331$ nm due to the aminophenol $\mathbf{1_{AP}}$. The spectra of these two species are similar, because the product imine $\mathbf{1_{PI}}^{\mathbf{Ph}}$ and aminophenol $\mathbf{1_{AP}}$ have the same skeleton of 6-amino-7-hydroxy indole chromophore. The reaction obeyed first-order kinetics in the presence of a large excess of benzylamine (1.8×10^{-1} M) as shown in the inset of Figure 11A. The pseudo-first-order rate constant was proportional to the amine concentration as shown in Figure 11B. Thus, the observed second-order rate constant k_4 was determined as 7.3×10^{-5} M^{-1} s^{-1} at 60 °C in methanol.

Electronic Effects of the Ether and Amino Groups on the Reactivity of 6,7-Indolequinones. The reaction of compound **2**, which has the ether substituent at C-4 (Chart 1), with benzylamine was also examined at 30 °C (Figure 12). In this case, the reaction was much slower as compared to those of compounds **1** and **4**. The observed second-order-rate constant was 2.3×10^{-2} M^{-1} s^{-1}, which was smaller than those of the reactions of **1** (4.1×10^{-2} M^{-1} s^{-1}) and **4** (2.7×10^{-1} M^{-1} s^{-1}) (Table 2). More importantly, the spectral change for the reaction of **2** (Figure 12A) is significantly different from those of the *iminoquinone* (IQ) *formation* of **1** (Figure 7A), but rather similar to the spectral change for the *productimine* (PI) *formation* of **1** shown in Figure 10A. Namely, spectrum (a) of quinone **2** at $\lambda_{max} = 384$ nm readily changed to spectrum (b), which was then gradually converted to spectrum (c) at $\lambda_{max} = 326$ nm with a clear isosbestic point at 374 nm. The final spectrum (c) is very close to the spectrum of product-imine $\mathbf{1_{PI}}^{\mathbf{Ph}}$ ($\lambda_{max} = 336$ nm) in Figure 10A [spectrum (d)]. Thus, the reaction of **2** and the amine at 30 °C resulted in formation of the corresponding product-imine $\mathbf{2_{PI}}^{\mathbf{Ph,H}}$ without accumulation of iminoquinone intermediate $\mathbf{2_{IQ}}^{\mathbf{Ph,H}}$ as shown in Scheme 6. The iminoquinone formation process from the quinone K_1k_2 must be much slower than the product-imine formation from the iminoquinone intermediate (k_3). This is also attributed to the higher electron-donor ability of the ether group as compared to the thioether substituent as clearly demonstrated by the redox potential $E°$ ($E°$ of **2** is more negative than that of **1** by ~100 mV, see Figure 6). Accordingly, quinone **3**, which has a more negative $E°$ value, hardly reacted with benzylamine in methanol *at 30 °C*.

To compare the reactivity of **2** and **3**, the reactions were examined at a higher temperature (60 °C). The observed second-order rate constants $k_{obs(2)}$ are summarized in Table 3. The $k_{obs(2)}$ value decreases with increasing the alkyl group of the amines (primary > secondary), and the amines with larger alkyl groups such as benzhydrylamine and *tert*-butylamine exhibit no reactivity toward **2** under the same reaction conditions (Table 3). In addition, the absence of kinetic deuterium isotope effect (KIE = 1.0) in the reaction of benzylamine ($PhCH_2NH_2$ vs $PhCD_2NH_2$; see Figure S13, Supporting Information) clearly indicates that the benzylic proton migration (k_3 process in Scheme 6) is not involved in the rate-determining step. The Hammett ρ constant of −0.74 obtained from the slope of the Hammett plot shown in Figure S14 in the Supporting Information (numerical data are presented in Table S4, Supporting Information) is very close to that of the iminoquinone formation process K_1k_2 of **1** ($\rho = -0.61$; see, Figure 9). This also supports the notion that the formation of $\mathbf{2_{IQ(6)}}^{\mathbf{R1,R2}}$ from **2** is rate-limiting.

As in the case of **1** (Scheme 5), the product imine $\mathbf{2_{PI}}^{\mathbf{Ph}}$ was further converted into an aminophenol product $\mathbf{2_{AP}}$ in the prolonged reaction time. The ESI-MS analysis of the resulting

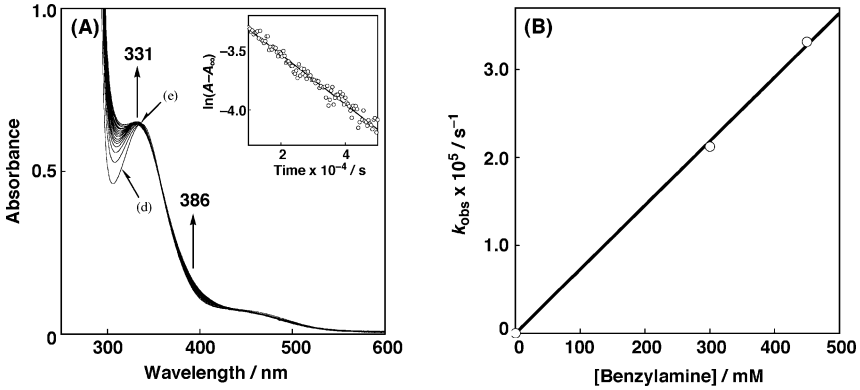

FIGURE 11. (A) Spectral changes for the formation of aminophenol $\mathbf{1_{AP}}$ from product imine $\mathbf{1_{PI}^{Ph}}$ generated by the reaction of **1** (5.0×10^{-5} M) and benzylamine (1.8×10^{-1} M) in CH_3OH at 60 °C. Inset: Pseudo-first-order plot for the aminophenol formation process. (B) Plot of $(10^5)k_{obs}$ vs [benzylamine].

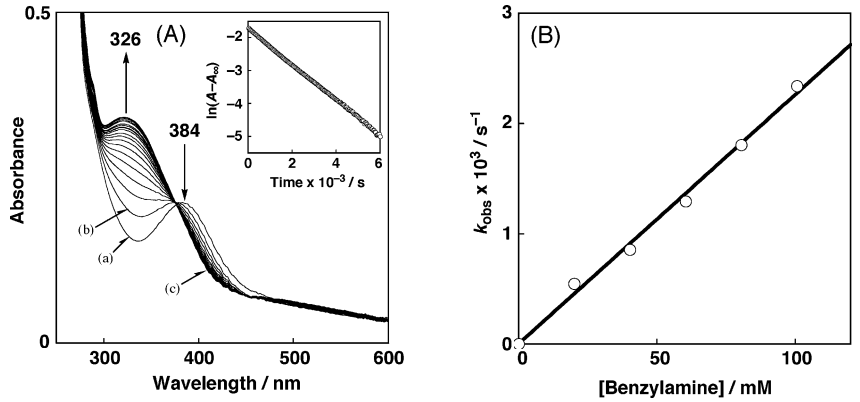

FIGURE 12. (A) Spectral change observed upon addition of benzylamine (2.0×10^{-2} M) to a CH_3OH solution of **2** (5.0×10^{-5} M) at 30 °C (isosbestic point, 374 nm). Inset: Pseudo-first-order plot for the product-imine formation. (B) Plot of the pseudo-first-order rate constants k_{obs} vs [benzylamine].

SCHEME 6

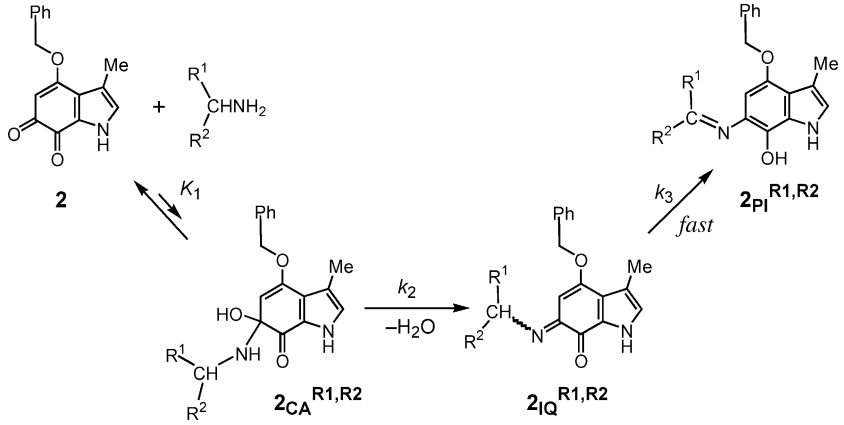

solution after 22 h at 60 °C clearly demonstrated the existence of distinct mass signals around *m*/*z* 267 and 291: the peak position agrees with the formulation of aminophenol $\mathbf{2_{AP}}$ (Figure S15, Supporting Information). The observed second-order rate constant k_4 was determined as 6.8×10^{-5} M^{-1} s^{-1} in methanol at 60 °C.

Similar results were obtained in the reaction of **3** and the amines, although reactivity of the quinone is much lower than that of compound **2**. For all amines, the reactivity of **3** is about (4−5)-fold lower than that of **2**. It was also confirmed that there was no kinetic deuterium isotope effect (KIE = 1.0) in the reaction with benzylamine ($PhCH_2NH_2$ and $PhCD_2NH_2$) (Figure S16, Supporting information). A similar Hammett ρ constant of −0.46 was obtained in the reaction with a series of para-substituted benzylamines (Figure S17, Supporting Information). These results support that the reaction of **3** and amines proceeds via the same mechanism as the rate-limiting iminoquinone formation process, as in the case of compound **2** shown in Scheme 6. The lower reactivity of **3** can be attributed to the stronger electron-donating nature of the amine substituent of **3**, which may depress the amine-addition to the C-6 quinone carbonyl group, thus decreasing the K_1 value.

TABLE 3. Observed Second-Order Rate Constants ($k_{obs(2)}$) for the Product-Imine Formation at 60 °C in Methanol and Their UV−Vis Data (λ_{max})[a]

	2		3	
amine	λ_{max}/ nm	$k_{obs(2)}$/ M^{-1} s^{-1}	λ_{max}/ nm	$k_{obs(2)}$/ M^{-1} s^{-1}
n-propylamine	337	0.14	340	0.029
benzylamine	326	0.074	339	0.015
cyclopropylamine	340	0.049	344	0.012
cyclohexylamine	336	0.028	341	0.0070
isopropylamine	331	0.019	339	0.0054
benzhydrylamine		*b*		*b*
tert-butylamine		*b*		*b*

[a] [Quinone] = 5.0×10^{-5} M, in CH_3OH, at 60 °C, under N_2. [b] Too slow to be determined accurately.

The product imine $\mathbf{3_{PI}^{Ph}}$ was further converted into an aminophenol product $\mathbf{3_{AP}}$ at the same condition ($k_4 = 1.5 \times 10^{-5}$ M^{-1} s^{-1}, the data are shown in Figure S18 and Figure S19 in the Supporting information). The reactivity of product imine $\mathbf{3_{PI(6)}^{Ph}}$ was also much lower than that of **1** and **2**, because of the stronger electron-donating nature and the steric repulsion of the methyl group of the amine substituent of **3**.

Summary and Conclusion

In this study, the electronic effects of the C-4 substituent on the physicochemical properties and reactivity of the 6,7-inodolequinone cofactors have extensively been investigated by using a series of C-4 substituted 6,7-inodolequinone derivatives **1**−**4** (Chart 1). The electron-donating ability of the C-4 substituent increases in the following order: indole (**4**) < thioether (**1**) < ether (**2**) < amine (**3**), as reflected in the redox potential $E^{o\prime}$ and the reactivity of the quinones with the amine substrates (Tables 2 and 3). The reaction of quinone compounds **1**−**3** with benzylamine proceeds stepwise through the iminoquinone (IQ) and the product-imine (PI) intermediates to give aminophenol (AP) as the final product as in the case of TTQ model compound **4**[27] and the TTQ-dependent enzymes.[37,38] However, the reactivity of CTQ model compound **1** toward the amines was by one order of magnitude lower than that of **4** (Table 2). This could be mainly attributed to the electron-donating effect of the sulfur substituent at C-4 of **1**. This disadvantage of CTQ in the amine-addition process (carbinolamine formation) could be overcome by modulating the electron-donor ability of the sulfur substituent by making a hydrogen-bonding interaction in the enzyme active site. However, there is no amino acid residue that can serve as a hydrogen-bonding donor to the sulfur atom of CTQ in the enzyme active site (the thioether group of CTQ is surrounded by hydrophobic amino acid residues).[21,22] Alternatively, the electrophilicity of the C-6 carbonyl carbon of CTQ toward the amine substrate could be enhanced by coordination of a Lewis acid to the carbonyl oxygen at C-6. In fact, there is a sodium cation interacting with the C-6 carbonyl oxygen in the enzyme active site as shown in Figure 13 (the distance between Na^+ and O(6) is 2.45 Å).[21] This may be an artifice to enhance the amine-addition process in the CTQ-dependent enzymes.[39]

Another important difference between CTQ and TTQ is the reactivity of the iminoquinone intermediate: the reaction of CTQ model compound **1** with amines stops at the iminoquinone formation stage *at room temperature* (Scheme 3), whereas the reaction of TTQ model compound **4** with the same amines proceeds up to the aminophenol formation under the same experimental conditions. This intriguing result clearly indicates that the energy barrier for the rearrangement of the iminoquinone to the product-imine (Scheme 4) is higher in the CTQ system than in the TTQ system. Thus, there must also be a trick to enhance the rearrangement process in the CTQ-dependent enzymes. An important clue for understanding this issue can be obtained by detailed inspection of the crystal structures of the phenylhydrazine-adduct of the enzymes.[38,40] In both enzymes, a carboxylate group of the active site aspartate (Asp128 in TTQ-dependent aromatic amine dehydrogenase[38] and Asp33 in CTQ-dependent quinohemoprotein amine dehydrogenase[40]) acts as a base to abstract a proton from the α-carbon of the added amine substrate. When the distance between the carboxylate oxygen of Asp and the α-nitrogen atom of the added phenylhydrazine (hydrazone derivative) is compared between these two systems, the distance in the CTQ-enzyme (2.77 Å) is apparently shorter than that in the TTQ-enzyme (2.82 Å) as indicated in Figure 14. Thus, the deprotonation from the α-position of the added substrate, required for the rearrangement from the iminoquinone to the product-imine, may be accelerated more sufficiently in the CTQ-dependent enzyme, which exhibits a shorter distance between the carboxylate oxygen and the α-position of the added substrate. This could be another artifice accommodated in the CTQ-enzymes.

The reactivity of the quinone with the ether substituent (compound **2**) toward amines is further retarded due to the

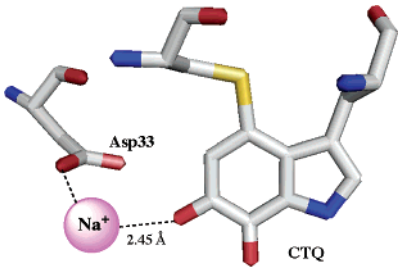

FIGURE 13. Active site structure of quinohemoprotein amine dehydrogenase.[21]

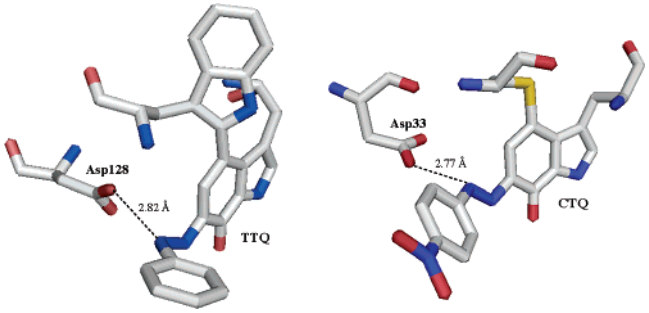

FIGURE 14. Active site structures of phenylhydrazine adduct of TTQ-dependent aromatic amine dehydrogenase (left)[38] and the *p*-nitrophenylhydrazine adduct of CTQ-dependent amine dehydrogenase (right).[40]

(37) Davidson, V. L. *Bioorg. Chem.* **2005**, *33*, 159−170.
(38) Masgrau, L.; Roujeinikova, A.; Johannissen, L. O.; Hothi, P.; Basran, J.; Ranaghan, K. E.; Mulholland, A. J. Sutcliffe, M. J.; Scrutton, N. S.; Leys, D. *Science* **2006**, *312*, 237−241.
(39) It has also been reported that there is a binding site of monovalent metal ion in the TTQ-dependent enzymes. However, the binding site for the metal ion has yet to be identified. Chen, L.; Doi, M.; Durley, R. C. E.; Chistoserdov, A. Y.; Lidstrom, M. E.; Davidson, V. L.; Mathews, F. S. *J. Mol. Biol.* **1998**, *276*, 131−149.
(40) Satoh, A.; Adachi, O.; Tanizawa, K.; Hirotsu, K. *Biochim. Biophys. Acta* **2003**, *1647*, 272−277.

higher electron donor ability of the oxygen substituent in **2** as compared to that of the sulfur substituent in **1**. The introduction of the amino group at C-4 of the quinone in **3** resulted in a further increase in the energy barrier for the iminoquinone formation process, thus lowering the observed second-order rate constant $k_{obs(2)}$ (Table 3). Thus, the 6,7-indolequinone having such C-4 substituents may not be able to serve as a redox cofactor in amine dehydrogenases.

Experimental Section

General. The reagents and the solvents used in this study were commercial products of the highest available purity and were further purified by the standard methods, if necessary.[41] CTQ model compound **1** and TTQ model compound **4** were obtained from previous studies.[26,29]

X-ray Structure Determination. The single crystals were mounted on a glass-fiber. Data of X-ray diffraction were collected by a Rigaku RAXIS-RAPID imaging plate two-dimensional area detector, using graphite-monochromated Mo Kα radiation (λ = 0.71069 Å) to $2\theta_{max}$ of 55.0°. All the crystallographic calculations were performed by using the Crystal Structure software package of the Molecular Structure Corporation [Crystal Structure: Crystal Structure Analysis Package version 3.5.1, Molecular Structure Corp. and Rigaku Corp. (2003)]. The crystal structures of compounds **3** and **8** were solved by direct methods and refined by full-matrix least-squares with SIR-92. All non-hydrogen atoms and hydrogen atoms were refined anisotropically and isotropically, respectively.

Electrochemical Measurement. Cyclic voltammetric measurements were performed on a BAS 50W potentiostat with a three-electrode system consisting of a glassy carbon electrode with ϕ = 3.0 mm (Bioanalytical System), a platinum plate auxiliary electrode, and an Ag|AgCl (saturated KC1) reference electrode. The glassy carbon electrode was polished with 0.05 μm alumina powder, sonicated to remove it, and washed with water. All electrochemical measurements were carried out at 25 °C under an atmospheric pressure of nitrogen, which was previously passed through a solution of the same composition as the electrolysis solution. An aliquot (5 μL) of a stock solution of compounds **1**, **2**, and **3** (ca.20 mM) in DMSO was injected into 1.0 mL of the electrolysis solutions containing 20% (v/v) isopropyl alcohol. All pH values of aqueous/organic mixed solvents were measured with a conventional pH meter and indicated without correction.

Kinetic Analysis. The reactions of the quinones and several amines were followed spectroscopically with a Hewlett-Packard 8453 photodiode array spectrophotometer under pseudo-first-order conditions with excess amine in deaerated CH_3OH. Typically, a CH_3OH solution of the quinone (5.0×10^{-5} M) was placed in a UV cell (1 cm path length, sealed tightly with a silicon rubber cap) and the solution was deaerated by bubbling N_2 through it for ca. 10 min. Then, an anaerobic stock solution of the amine was added with use of a microsyringe to start the reaction. The pseudo-first-order rate constant was determined from the rate of a decrease in intensity of the absorption due to the quinone or an increase in intensity of the absorption due to the product. The nonlinear curve-fitting program was used to determine the rate constants when the final value of the absorbance (A_∞) was obscured by the follow-up reaction.

Product Analysis: (i) Reaction with Cyclopropylamine. A methanol solution of **1** (5.0×10^{-5} M) was placed in a UV cell (1 cm pass length, sealed tightly with a silicon rubber cap) and the solution was deaerated by bubbling N_2 through it for ca. 10 min. Then cyclopropylamine (50 equiv) was introduced into the solution with a microsyringe to start the reaction at 30 °C. The reaction products were analyzed by ESI-MS.

(41) Perrin, D. D.; Armarego, W. L. F.; Perrin, D. R., *Purification of Laboratory Chemicals*, 4th ed.; Pergamon Press: Elmsford, NY, 1996.

(ii) Reaction with Benzylamine. The reactions of **1**−**3** and benzylamine were performed similarly but at 60 °C, and the products were analyzed by ESI-MS.

(iii) Theoretical Calculations. Density-functional theory (DFT) calculations were performed on an 8 CPU workstation (PQS, Quantum Cube QS8-2400C-064). Geometry optimizations were carried out with the Becke3LYP functional and 6-31G(d) basis set,[42] with the restricted Hartree−Fock (RHF) formalism and as implemented in the Gaussian 03 program Revision C.02.[43]

Synthesis: 4-Benzyloxy-3-methylindole-6,7-dione (2). 3-Methyl-1-*p*-tosylindole-6,7-dione (**7**) was prepared from vanillin via 11 steps according to the reported procedures.[29,44,45] Benzyl alcohol (13.5 μL, 0.13 mmol) and potassium *tert*-butoxide (14.4 mg, 0.13 mmol) were suspended in dry CH_3CN (5.0 mL) at room temperature under N_2, and the mixture was stirred for 1 h. A dry CH_3CN (10.0 mL) solution of **7** (40.0 mg, 0.13 mmol) was then added to the mixture, and the resulting solution was stirred at 25 °C for 6 h. The reaction mixture was then diluted with water (30 mL), extracted with ethyl acetate (20 mL × 3), and dried over $MgSO_4$. After removing $MgSO_4$ by filtration, evaporation of the solvent gave a dark brown solid, from which compound **2** was isolated as a dark brown solid in a 23% conversion yield by SiO_2 column chromatography ($CHCl_3$) under air. Single crystals of this compound were obtained by recrystallization from CH_2Cl_2/hexane: IR (KBr) 1662, 1631 cm^{-1} (C═O); ^1H NMR ($CDCl_3$) δ 2.20 (s, 3 H), 5.13 (s, 2 H), 5.59 (s, 1 H), 6.88 (s, 1 H), 7.26−7.43 (m, 5 H); HRMS (FAB) *m*/*z* 268.0968 ([M + 1]$^+$) calcd for $C_{16}H_{13}NO_3$ 268.0974. Anal. Calcd for $C_{16}H_{13}NO_3$ + (1/4)H_2O: C, 70.71; H, 5.01; N, 5.15. Found: C, 70.68; H, 4.85; N, 5.02.

4-(*N*-Methylbenzylamino)-3-methyl-1-*p*-tosylindole-6,7-dione (8). To a dry CH_3CN solution (6.0 mL) of **7** (30.0 mg, 0.095 mmol) was added *N*-methylbenzylamine (12 μL, 0.095 mmol) at room temperature under N_2, and the resulting mixture was stirred at room temperature for 2 day. The reaction mixture was then diluted with water (30 mL), extracted with ethyl acetate (20 mL × 3), and dried over $MgSO_4$. After $MgSO_4$ was removed by filtration, evaporation of the solvent gave a purplish red solid, from which compound **8** was isolated as a red solid in a 95% conversion yield by SiO_2 column chromatography ($CHCl_3$) under air. Single crystals of this compound were obtained by recrystallization from CH_2Cl_2/hexane: IR (KBr) 1680, 1616 (C═O), 1375 and 1178 cm^{-1} (SO_2); ^1H NMR ($CDCl_3$) δ 2.30 (s, 3 H), 2.42 (s, 3 H), 2.72 (s, 3 H), 4.40 (s, 2 H), 5.55 (s, 1 H), 7.16−7.34 (m, 7 H), 7.69 (s, 1 H), 8.09 (d, J = 8.3 Hz, 2 H); HRMS (FAB) *m*/*z* 435.1382 ([M + 1]$^+$) calcd for $C_{24}H_{22}N_2O_4S$ 435.1378. Anal. Calcd for $C_{24}H_{22}N_2O_4S$ + (1/3)H_2O: C, 65.44; H, 5.19; N, 6.36. Found: C, 65.16; H, 5.02; N, 6.40.

4-(*N*-Methylbenzylamino)-3-methylindole-6,7-dione (3). To a suspension of **8** (40.0 mg, 0.092 mmol) in dry CH_3CN (15.0 mL, deoxygenated by bubbling N_2 for 10 min) was added methylhydrazine (45 μL, 0.855 mmol, 9.3 equiv), and the reaction mixture was stirred for 2 days under anaerobic conditions (N_2). Removal of the solvent under reduced pressure gave a yellow solid material (**8H$_2$**), to which 3 N NaOH in H_2O−EtOH (1.1 mL, 9:5, v/v) was added. The mixture was then stirred at room temperature for 10 min and then extracted with ethyl acetate (15 mL × 6). After the extract was dried over $MgSO_4$, evaporation of the solvent gave a dark red residue, from which compound **3** was isolated in 72% yield by column chromatography (SiO_2, $CHCl_3$): IR (KBr) ~3275

(42) (a) Becke, A. D. *J. Chem. Phys.* **1993**, *98*, 5648. (b) Lee, C.; Yang, W.; Parr, R. G. *Phys. Rev. B* **1988**, *37*, 785−789. (c) Hehre, W. J.; Radom, L.; Schleyer, P. v. R.; Pople, J. A. *Ab Initio Molecular Orbital Theory*; Wiley: New York, 1986.

(43) Frisch, M. J.; et al. *Gaussian 03*, Revision C.02; Gaussian, Inc.: Wallingford CT, 2004.

(44) Benington, F.; Morin, R. D.; Clark, L. C., Jr. *J. Org. Chem.* **1959**, *24*, 917−919.

(45) Magnus, P.; Gazzard, L.; Hobson, L.; Payne, A. H.; Rainey, T. J.; Westlund, N.; Lynch, V. *Tetrahedron* **2002**, *58*, 3423−3443.

(br N−H), 1661, 1595 cm^{-1} (C═O); ^1H NMR ($CDCl_3$) δ 2.26 (s, 3 H), 2.80 (s, 3 H), 4.53 (s, 2 H), 5.53 (s, 1 H), 7.02 (s, 1 H), 7.22−7.36 (m, 5 H), 10.2 (br s, 1 H); HRMS (FAB) *m*/*z* 281.1301 ($[M + 1]^+$) calcd for $C_{17}H_{17}O_2N_2$ 281.1290. Anal. Calcd for $C_{16}H_{13}O_2N_2 + (1/4)H_2O$: C, 71.69; H, 5.84; N, 9.84. Found: C, 71.63; H, 5.68; N, 9.73.

Acknowledgment. This work was financially supported in part by Grants-in-Aid for Scientific Research (Nos. 17350086, 18037062, and 18033045 for S.I.) from the Ministry of Education, Culture, Sports, Science and Technology, Japan.

Supporting Information Available: IR spectra of **1**−**4** (Figures S1−S4), spectroscopic pH titration data of **1** (Figure S5), kinetic analysis data for the reactions of the quinones and the amines (Figures S6−S9, S13, S14, and S16−S18 and Tables S3 and S4), ESI-MS data of the products (Figures S10−S12, S15, S19), and ^1H NMR spectra of **2**, **8**, and **3** (Figures S20−S22); details of the crystallographic data for compounds **3** and **8** (Tables S1 and S2, and CIF format data). This material is available free of charge via the Internet at http://pubs.acs.org.

JO0700272